DOI: 10.3969/j.issn.1673-3185.2017.05.008 **http**: // english.ship-research.com

Translated from: YE L Y, WANG C, LI P, et al. Calculation of marine propeller static strength based on coupled BEM/FEM[J]. Chinese Journal of Ship Research, 2017, 12(5): 64-74, 83.

Calculation of marine propeller static strength based on coupled BEM/FEM

YE Liyu, WANG Chao, LI Peng, WANG Xidong

College of Shipbuilding Engineering, Harbin Engineering University, Harbin 150001, China

Abstract: [**Objectives**] The reliability of propeller stress has a great influence on the safe navigation of a ship. To predict propeller stress quickly and accurately, [**Methods**] a new numerical prediction model is developed by coupling the Boundary Element Method (BEM) with the Finite Element Method (FEM). The low order BEM is used to calculate the hydrodynamic load on the blades, and the Prandtl-Schlichting plate friction resistance formula is used to calculate the viscous load. Next, the calculated hydrodynamic load and viscous correction load are transmitted to the calculation of the Finite Element as surface loads. Considering the particularity of propeller geometry, a continuous contact detection algorithm is developed; an automatic method for generating the finite element mesh is developed for the propeller blade; a code based on the FEM is compiled for predicting blade stress and deformation; the DTRC 4119 propeller model is applied to validate the reliability of the method; and mesh independence is confirmed by comparing the calculated results with different sizes and types of mesh. [**Results**] The results show that the calculated blade stress and displacement distribution are reliable. This method avoids the process of artificial modeling and finite element mesh generation, and has the advantages of simple program implementation and high calculation efficiency. [**Conclusions**] The code can be embedded into the code of theoretical and optimized propeller designs, thereby helping to ensure the strength of designed propellers and improve the efficiency of propeller design.

Key words: propeller; strength prediction; Boundary Element Method (BEM); Finite Element Method (FEM); stress distribution

CLC number: U664.33

0 Introduction

As the power source in the navigation process of ship, propeller has always been an important focus of ship design. The reliability of propeller structure is the prerequisite to ensure that the navigational performance of ship meets the requirements, so it is of great significance to the safety of navigation. However, with the development of ship towards large size and high speed, the application of high-power main engine leads to the increased surface load of propeller blades, and the wide application of highly skewed propeller makes the strength problem of propeller more prominent. When a propeller works, the thrust and rotational resistance of the propeller exert bending and twisting effects on the blades, and the centrifugal force produced by the propeller rotation will cause the blades to bend and stretch outwards. If the propeller strength is not enough, the propeller may be damaged or broken, or the hydrodynamic performance of the propeller cannot meet the design requirements due to the large deformation. Therefore, in order to improve the efficiency of propeller design and ensure the strength of propeller blades, it is urgent to develop a method that can accurately and rapidly predict the strength of propeller blades.

At present, the methods of specification check, numerical prediction and model test can be used for

Received: 2017 - 03 - 28

Supported by: Fund of National Ministries and Commissions; National Natural Science Foundation of China (51679052)

Author(s): YE Liyu, male, born in 1989, Ph.D. candidate. Research interest: design and performance evaluation of ship propeller in ice zone. E-mail: yeliyuxrxy@126.com

WANG Chao (Corresponding author), male, born in 1981, Ph.D., associate professor. Research interest: ship propulsion and vibration and noise reduction technology, and ice zone propulsion technology. E-mail: wangchao0104@hrbeu.edu.cn

the prediction of propeller blade strength. The methods and requirements of strength check are stipulated in the specifications in China and abroad, but they were proposed mainly based on a great deal of usage experience, and the prediction results are conservative. In the aspect of model test, Boswell [1] conducted static stress measurement test for the blades of highly skewed propeller; Zhao [2] carried out static stress test and dynamic stress test of highly skewed propeller, which were compared with the theoretical calculation results; Yang et al. [3] studied the strain and stress distribution of blades under different operating conditions by sticking strain gages on the surface of highly skewed propeller model. It can be seen from the above research and test results that, the cost of the propeller strength model test is higher, and the test is difficult and time-consuming, which cannot be widely used.

The numerical analysis method of propeller strength mainly adopts the cantilever beam method and the finite element method (FEM). The cantilever beam method is a relatively convenient and feasible method for predicting the blade stress, but this method simplifies the blades to a twisty cantilever beam of variable cross section, and this defect makes it impossible to predict the strength of propeller accurately [4]. For the FEM, the commonly used method is to predict the stress distribution of blades using the method that combines CFD calculation with finite element analysis software [5-6]. There are also some scholars link up the boundary element method (BEM) and finite element analysis software for the prediction of blade stress distribution [7-8]. Although this method can accurately predict the stress distribution of propeller blades, it requires complex modeling and meshing process, which is not conducive to the propeller design, and the problem of inadequate interface stability also exists in the linkup of BEM program and finite element software. Some scholars made their own finite element programs to carry out calculation of the propeller strength. For example, Hu et al. [9] regarded the propeller blades as thick shell elements, split the blades into 12 elements, and programmed the corresponding stress analysis program; Wang [10] developed finite element program HPROP of strength calculation specifically for highly skewed propeller, where the pressure value calculated by the lifting surface method was input into the finite element program for calculation; Liu et al. [11] calculated the propeller strength under hydrodynamic load by combining BEM program and finite element calculation program HPROP. For the strength calculation using the finite element programs developed on their own, the above references did not introduce the specific implementation process in detail. From the calculation diagrams, they have some limitations in the division of finite element structural elements of solid propeller, and the number of structural elements is small, which may bring about the problem of insufficient calculation accuracy.

In this paper, the propeller strength calculation method based on coupled BEM/FEM was studied, and a method for the accurate and fast prediction of propeller strength was proposed, which provides an approach for the evaluation of propeller strength at the design stage. Overall, this method is to transfer the propeller surface pressure calculated by BEM to the finite element structure calculation of propeller. The problem addressed here is how to establish an automatic division method for finite element structural elements in the case of fixed meshing of the propeller surface, so as to achieve the transfer of hydrodynamic load between two methods. To this end, the relevant theory of propeller strength calculation using FEM and the specific numerical calculation process were detailed in this paper. The program for propeller strength prediction by FEM was compiled using Fortran language, which was linked up with the performance prediction program of steady BEM of propeller. Finally, taking blade strength prediction of a propeller as an example, the validity of the method proposed in this paper was verified.

1 Theory of BEM

The BEM of propeller does not make any assumptions about the shape of objects. It satisfies the boundary conditions on the real object surfaces and can predict the hydrodynamic performance of propeller accurately, so it has been widely used in recent years.

The rectangular coordinate system $O-XYZ$ and cylindrical coordinate system $O-XR\theta$ fixed on the blades are shown in Fig. 1. In the figure, R and θ are the radial coordinate vector and angular coordinate vector respectively. Assuming that the propeller rotates by an angular velocity ω in the case of the inflow velocity of V_0, using the Green formula, the Laplasse equation for describing the incompressible, inviscid and irrotational potential flow problems was transformed into integral equations on the object boundary, so that the problem of flow around object was transformed into the calculation of unknown node strength on any surface [12].

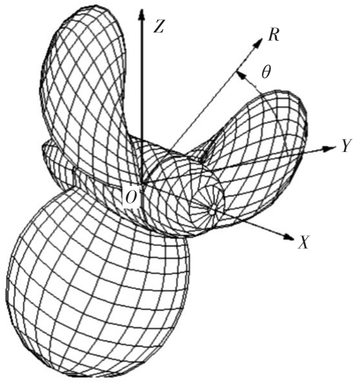

Fig.1 Ccoordinates of propeller

$$2\pi\phi(P)=\iint_{S_B}\phi(Q)\frac{\partial}{\partial \boldsymbol{n}_Q}(\frac{1}{R_{PQ}})\mathrm{d}S+$$

$$\iint_{S_W}\Delta\phi(Q_1)\frac{\partial}{\partial \boldsymbol{n}_{Q1}}\frac{1}{R_{PQ_1}}\mathrm{d}S+\iint_{S_B}(V_0\cdot\boldsymbol{n}_Q)(\frac{1}{R_{PQ}})\mathrm{d}S \quad (1)$$

In the formula: S_W is the trailing vortex surface; ϕ is perturbation velocity potential; R_{PQ} and R_{PQ_1} are distances from field point P to point Q on the propeller surface and to point Q_1 on the trailing vortex surface, respectively; $\boldsymbol{n}_Q$ and $\boldsymbol{n}_{Q1}$ are the unit normal vectors of point Q on the propeller surface and point Q_1 on the trailing vortex surface, respectively; $\Delta\phi$ is the velocity potential jump through the trailing vortex surface S_W which can be expressed in S_W as

$$\Delta\phi=\phi^+-\phi^- \quad (2)$$

In the formula, superscripts "+" and "−" represent the values on the upper and lower surfaces of the trailing vortex surface, respectively.

For the steady problem of propeller, velocity potential jump $\Delta\phi$ of trailing vortex surface was a constant at the same radius. The equivalence between normal dipole distribution and vortex ring distribution shows that, $\Delta\phi$ is the trailing vortex strength, which can be determined by meeting the Kutta conditions at the trailing edge of lifting body. There are many forms of Kutta conditions, and the pressure Kutta condition was used here, which requires that the pressure difference $(\Delta p)_{\mathrm{TE}}$ of the upper and lower surfaces at the trailing edge of lifting body was 0, namely,

$$(\Delta p)_{\mathrm{TE}}=p^+_{\mathrm{TE}}-p^-_{\mathrm{TE}}=0 \quad (3)$$

In the formula, subscript TE refers to the following edge of propeller.

Combined with the Kutta conditions, the numerical solution of the linear equations can be solved iteratively, namely, perturbation velocity potential ϕ of object surface. The velocity on the object surface can be determined by the velocity potential on the object surface by using the method developed by Yanagisawa, and then the pressure on the propeller surface can be calculated by Bernoulli equation.

2 Calculation of propeller strength by FEM

2.1 Automatic finite element meshing method of propeller

FEM divides the complex solution region of continuous medium into a group of elements with finite number and connected together in a certain way. Therefore, meshing is one of the key technologies of finite element analysis, and also the most time-consuming work with the largest volume in the process of preparing the finite element data, so it has been paid great attention in the development process of finite element technique. In this section, we focused on the automatic finite element meshing method of propeller. After the program compilation, the users only need to input the offset table of propeller to achieve the automatic completion of body elements of propeller finite element structure on the computer. This method is simple to use, reliable in performance and generates the elements of good quality.

Because the geometry of the propeller is complex, in order to generate the node coordinates of the structural elements, it is necessary to make the geometric expression of the coordinates of the blade surface first. In the cylindrical coordinate system in Fig. 2, s_1 is the chord-wise distance between a point on the blade section and the leading edge, c_1 is the distance between the leading edge on the blade section and the generatrix, x_r is the pitching of the blade section, θ_s is skew angle of the section, β is the geometric pitch angle of the propeller, y_b and y_f are distances from the points on the blade back and the blade surface to chord, respectively, and subscripts b and f represent the blade back and surface of the propeller. In the cylindrical coordinate system $O-XR\theta$, the coordinates of the points on the blade section at radius R of the propeller can be expressed as

$$\begin{cases} x=x_r+(-c_1+s_1)\sin\beta-\begin{pmatrix} y_b \\ y_f \end{pmatrix} \\ R=R \\ \theta=\dfrac{1}{R}\left[(-c_1+s_1)\cos\beta\begin{pmatrix} y_b \\ y_f \end{pmatrix}\sin\beta\right]+\theta_s \end{cases} \quad (4)$$

The corresponding coordinates in the coordinate

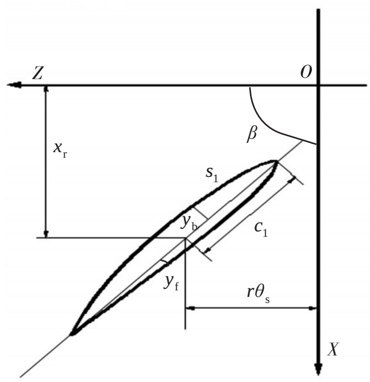

Fig.2 Expression of blade section

system $O-XYZ$ are

$$\begin{cases} x = x_r + (-c_1 + s_1)\sin\beta - \begin{pmatrix} y_b \\ y_f \end{pmatrix}\cos\beta \\ y = R\cos\theta \\ z = R\sin\theta \end{cases} \tag{5}$$

In the BEM calculation, the propeller surface was divided into a series of small elements, and each element was replaced by a hyperboloid element, as shown in Fig. 3. Here, cosine division was used in the chord-wise and span-wise directions, and the span-wise node r_j is represented as

$$r_j = \frac{1}{2}(R_0 + r_h) - \frac{1}{2}(R_0 - r_h)\cos\beta_{rj}$$
$$j = 1, 2, \cdots, N_r + 1 \tag{6}$$

The chord-wise node s_i is expressed as

$$s_i = \frac{1}{2}(1 - \beta_{ci})b_j\,;\ i = 1, 2, \cdots, N_c + 1 \tag{7}$$

In the formulas: R_0 and r_h are propeller radius and hub radius respectively; b_j is chord length of blade section at r_j; N_r and N_c are the span-wise and chord-wise mesh numbers respectively; β_{rj} and β_{ci} are the span-wise node angle and chord-wise node angle, respectively, which are expressed as follows:

$$\beta_{rj} = \begin{cases} 0 & ;\quad j = 1 \\ \dfrac{2j-1}{2N_r + 1}\pi; & j = 2, \cdots, N_r + 1 \end{cases} \tag{8}$$

$$\beta_{ci} = \frac{i-1}{N_c}\pi;\quad i = 1, 2, \cdots, N_c + 1 \tag{9}$$

Considering the particularity of the propeller structure, the solid structure of the propeller was meshed along the span-wise direction, chord-wise direction and thickness direction, forming the 8-node hexahedron elements as shown in Fig. 3. In order to better link up the prediction program of BEM, so that the hydrodynamic load can be transferred to the calculation of finite element structure, the span-wise and chord-wise meshing of the blades was the same with that of BEM. Thus, the node coordinates of the finite element solid structure of propeller on the outer layer coincided with those of the surface mesh nodes of BEM. Cosine division was used here for chord-wise and span-wise directions, and the main purpose is to refine the leading edge/following edge and blade root / blade tip to reflect the geometric features of these regions. Average division was used for the thickness direction of the blades.

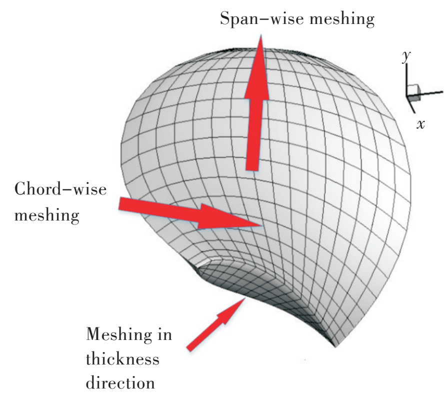

Fig.3 FE mesh model of propeller blade

Compared with tetrahedron, hexahedral element has better convergence, and the number of hexahedral elements and nodes needed for the same precision is much smaller than that of tetrahedral element[13]. Not only the analysis results of solid meshed by tetrahedral element are better than those by tetrahedral element, but also the discrete number of elements is also much smaller than that of tetrahedral element[14]. In addition, hexahedral element has the advantage of being easier to be identified from the geometric shape. Therefore, the researchers are willing to use hexahedral element to complete the finite element analysis of three-dimensional solid. Through the meshing in span-wise, chord-wise and thickness directions of the propeller solid structure, except the leading edge and the following edge, other parts were meshed into 8-node hexahedron, and the leading edge and following edge were meshed into pentahedral elements. The lines on the leading edge of the pentahedral elements were taken as the case that spatial quadrangle degenerated into a straight line segment, which still can be regarded as 8-node hexahedron in FEM calculation, as shown in Fig. 4.

2.2 Global stiffness matrix and equilibrium equation of force

From the above section we can see that, considering the particularity of propeller structure in this paper, the 8-node hexahedral element was used to

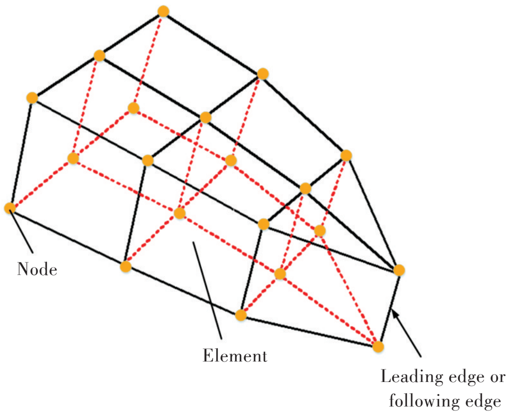

Fig.4 Generation of the hexahedral element

mesh the solid structure of propeller. Here, the 8-node hexahedral element was taken as an example to introduce the related theory of FEM.

For the propeller under the hydrodynamic loads in the rotating coordinate system, the overall dynamic equation of finite element structure can be expressed as

$$\boldsymbol{M}\ddot{\boldsymbol{u}} + \boldsymbol{C}\dot{\boldsymbol{u}} + \boldsymbol{K}\boldsymbol{u} = \boldsymbol{F}_{\mathrm{ce}} + \boldsymbol{F}_{\mathrm{co}} + \boldsymbol{F}_{\mathrm{r}} \tag{10}$$

In the formula: $\boldsymbol{M}$, $\boldsymbol{C}$ and K are the overall additional inertia force matrix, additional damping force matrix and stiffness matrix, respectively; $\ddot{\boldsymbol{u}}$, $\dot{\boldsymbol{u}}$, $\boldsymbol{u}$ are respectively the acceleration, velocity and displacement of nodes; $\boldsymbol{F}_{\mathrm{ce}}$, $\boldsymbol{F}_{\mathrm{co}}$ and $\boldsymbol{F}_{\mathrm{r}}$ are the centrifugal force, Coriolis force and hydrodynamic load respectively.

For a propeller in uniform flow, when it rotates at a fixed speed, the hydrodynamic load on it is steady load. The acceleration $\ddot{\boldsymbol{u}}$, velocity $\dot{\boldsymbol{u}}$ and Coriolis force $\boldsymbol{F}_{\mathrm{co}}$ of the nodes were 0. Then, Formula (10) can be simplified to

$$\boldsymbol{K}\boldsymbol{u} = \boldsymbol{F}_{\mathrm{ce}} + \boldsymbol{F}_{\mathrm{r}} \tag{11}$$

Because FEM meshes the solid structure into elements, stiffness of all elements can be integrated and superimposed to obtain the global stiffness matrix $\boldsymbol{K}$. The total nodal force matrix $\boldsymbol{F} = \boldsymbol{F}_{\mathrm{ce}} + \boldsymbol{F}_{\mathrm{r}}$ was obtained by the integration and superposition of equivalent nodal force of all elements. Formula (11) can be discretized into a large linear system of equations, and the unknown nodal displacement and nodal force can be obtained by combining the known displacement boundary conditions and force boundary conditions.

The calculated nodal force can be transformed to the equivalent stress $\bar{\sigma}$ (Von-Mises stress) by Formula (12).

$$\bar{\sigma} = \frac{1}{\sqrt{2}}\sqrt{(\sigma_x-\sigma_y)^2+(\sigma_y-\sigma_z)^2+(\sigma_z-\sigma_x)^2+6(\tau_{xy}^2+\tau_{yz}^2+\tau_{zx}^2)} \tag{12}$$

In the formula: σ_x , σ_y , σ_z are the normal stress in the x, y, z directions, respectively; τ_{xy} is shear stress in the x direction on the normal surface and parallel to the y axis; τ_{yz} is shear stress in the y direction on the normal surface and parallel to the z axis; τ_{zx} is shear stress in the z direction on the normal surface and parallel to the x axis.

2.3 Basic equation and stiffness matrix of element

The basic equations of element in the spatial problems can be deduced by the principle of virtual displacement and the virtual work equation [15].

$$\boldsymbol{K}^{\mathrm{e}}\boldsymbol{u}^{\mathrm{e}} = \boldsymbol{F}^{\mathrm{e}} \tag{13}$$

In the formula, $\boldsymbol{K}^{\mathrm{e}}$ is the stiffness matrix of spatial element, and the superscript e represents element; $\boldsymbol{u}^{\mathrm{e}}$ is the displacement array of element node; and $\boldsymbol{F}^{\mathrm{e}}$ is the equivalent nodal force array of element. The calculation method will be introduced in section 2.4.

The stiffness matrix $\boldsymbol{K}^{\mathrm{e}}$ of spatial element can be expressed as

$$\boldsymbol{K}^{\mathrm{e}} = \iiint_V \boldsymbol{B}^{\mathrm{eT}}\boldsymbol{D}^{\mathrm{e}}\boldsymbol{B}^{\mathrm{e}}\mathrm{d}x\mathrm{d}y\mathrm{d}z \tag{14}$$

In the formula, $\boldsymbol{D}^{\mathrm{e}}$ is the elastic matrix of element; $\boldsymbol{B}^{\mathrm{e}}$ is the strain matrix of element, and the form of block matrix is written as follows

$$\boldsymbol{B}^{\mathrm{e}} = \boldsymbol{B}_1\boldsymbol{B}_2\boldsymbol{B}_3\boldsymbol{B}_4\boldsymbol{B}_5\boldsymbol{B}_6\boldsymbol{B}_7\boldsymbol{B}_8 \tag{15}$$

where,

$$\boldsymbol{B}_i = \begin{bmatrix} \frac{\partial N_i}{\partial x} & 0 & 0 & \frac{\partial N_i}{\partial y} & 0 & \frac{\partial N_i}{\partial z} \\ 0 & \frac{\partial N_i}{\partial y} & 0 & \frac{\partial N_i}{\partial x} & \frac{\partial N_i}{\partial z} & 0 \\ 0 & 0 & \frac{\partial N_i}{\partial z} & 0 & \frac{\partial N_i}{\partial y} & \frac{\partial N_i}{\partial x} \end{bmatrix}$$

$$i = 1, \cdots, 8 \tag{16}$$

In the formula, N_i is the interpolation function; $\partial N_i/\partial x$, $\partial N_i/\partial y$, $\partial N_i/\partial z$ are respectively expressed as follows:

$$\begin{cases} \frac{\partial N_i}{\partial x} = \frac{\xi_i}{8a}(1+\eta_i\eta)(1+\zeta_i\zeta); \quad i=1,2,\cdots,8 \\ \frac{\partial N_i}{\partial y} = \frac{\eta_i}{8a}(1+\zeta_i\zeta)(1+\xi_i\xi); \quad i=1,2,\cdots,8 \\ \frac{\partial N_i}{\partial x} = \frac{\xi_i}{8a}(1+\xi_i\xi)(1+\eta_i\eta); \quad i=1,2,\cdots,8 \end{cases} \tag{17}$$

where a is the side length of element; ξ , η and

ζ are local coordinate systems of isoparametric element.

The elastic matrix $\boldsymbol{D}^{\mathrm{e}}$ of element is a constant matrix determined by the elastic modulus E and Poisson's ratio μ, which is obtained by Formula (18).

$$\boldsymbol{D}^{\mathrm{e}}=\frac{E}{(1+\mu)(1-2\mu)}\begin{bmatrix}1-\mu & \mu & \mu & 0 & 0 & 0\\ \mu & 1-\mu & \mu & 0 & 0 & 0\\ \mu & \mu & 1-\mu & 0 & 0 & 0\\ 0 & 0 & 0 & \frac{1-2\mu}{2} & 0 & 0\\ 0 & 0 & 0 & 0 & \frac{1-2\mu}{2} & 0\\ 0 & 0 & 0 & 0 & 0 & \frac{1-2\mu}{2}\end{bmatrix} \tag{18}$$

Formula (18) was deduced in the condition of regular element structure. For the 8-node hexahedral element, Formula (18) was only suitable for the calculation of regular hexahedral element. Due to the complicated structure of the propeller, the hexahedron obtained by meshing the solid structure of the propeller was irregular, and it is necessary to introduce isoparametric elements for coordinate transformation. After the coordinate transformation of isoparametric element, the general expression of element stiffness matrix in the local coordinate system (ξ, η, ζ) was obtained.

$$\boldsymbol{K}^{\mathrm{e}}=\iiint_V \boldsymbol{B}^{\mathrm{eT}}\boldsymbol{D}^{\mathrm{e}}\boldsymbol{B}^{\mathrm{e}}|\boldsymbol{J}|\mathrm{d}\xi\mathrm{d}\eta\mathrm{d}\zeta \tag{19}$$

In the formula, $|\boldsymbol{J}|$ is Jacobian determinant. The Jacobian matrix $\boldsymbol{J}$ of the 8-node hexahedral element can be expressed as

$$\boldsymbol{J}=\begin{bmatrix}\sum_{i=1}^{8}\frac{\partial N_i}{\partial\xi}x_i & \sum_{i=1}^{8}\frac{\partial N_i}{\partial\xi}y_i & \sum_{i=1}^{8}\frac{\partial N_i}{\partial\xi}z_i\\ \sum_{i=1}^{8}\frac{\partial N_i}{\partial\eta}x_i & \sum_{i=1}^{8}\frac{\partial N_i}{\partial\eta}y_i & \sum_{i=1}^{8}\frac{\partial N_i}{\partial\eta}z_i\\ \sum_{i=1}^{8}\frac{\partial N_i}{\partial\zeta}x_i & \sum_{i=1}^{8}\frac{\partial N_i}{\partial\zeta}y_i & \sum_{i=1}^{8}\frac{\partial N_i}{\partial\zeta}z_i\end{bmatrix} \tag{20}$$

2.4 Non-node load shifting

After the structure was discretized, each element was connected by nodes, the displacement of the structure was approximately represented by the displacement of all nodes, and their external loads should be shifted equivalently to the element nodes for the analysis of element characteristics. According to principle of virtual displacement of elastic mechanics, external loads can be shifted onto the element nodes.

If there was a concentrated force $\boldsymbol{P}^{\mathrm{e}}=\left\{P_x, P_y, P_z\right\}^{\mathrm{eT}}$ within element e, according to the principle of virtual displacement, the equivalent nodal force matrix after the shifting can be obtained:

$$\boldsymbol{F}_P^{\mathrm{e}}=\boldsymbol{N}^{\mathrm{T}}\boldsymbol{P}^{\mathrm{e}} \tag{21}$$

In the formula, $\boldsymbol{N}$ is the shape function matrix. The propeller was not affected by concentrated force, and this force was set to 0.

If there was element volume force $\boldsymbol{G}^{\mathrm{e}}=\left\{G_x, G_y, G_z\right\}^{\mathrm{eT}}$ within element e, the volume force Gdxdydz on differential volume dxdydz was taken as the concentrated force, and we can get the equivalent nodal force matrix after the shifting:

$$\boldsymbol{F}_G^{\mathrm{e}}=\iiint_V \boldsymbol{N}^{\mathrm{T}}\boldsymbol{G}^{\mathrm{e}}\mathrm{d}x\mathrm{d}y\mathrm{d}z \tag{22}$$

The propeller would cause centrifugal force due to the rotation effect, which can be treated as a volume force, and the calculation formula is

$$\boldsymbol{F}_{\mathrm{ce}}^{\mathrm{e}}=\iiint_V \rho\boldsymbol{N}^{\mathrm{T}}\{-\omega\times(\omega\times\boldsymbol{X})\}\mathrm{d}x\mathrm{d}y\mathrm{d}z \tag{24}$$

In the formula: ρ is material density of the propeller; ω is the rotational angular velocity of the propeller; $\boldsymbol{X}$ is node coordinate vector. If there was surface force $\bar{\boldsymbol{P}}=\left\{\bar{P}_x, \bar{P}_y, \bar{P}_z\right\}^{\mathrm{T}}$ distributed on an interface of element e, taking the force $\bar{\boldsymbol{P}}\cdot\mathrm{d}A$ (A is the element area) on the differential surface dA as the concentrated force, we can get the equivalent nodal force matrix after the shifting

$$\boldsymbol{F}_{\bar{p}}^{\mathrm{e}}=\iint_A \boldsymbol{N}^{\mathrm{T}}\bar{\boldsymbol{P}}^{\mathrm{e}}\mathrm{d}A \tag{25}$$

For the propeller, it is mainly the effect of hydrodynamic load and viscous resistance on the blades during propeller rotation. Based on the automatic finite element meshing method established in this paper, the outer surface element of the finite element solid structure of the propeller can be coincident with the surface element of BEM. Therefore, the pressure distribution at the surface element center of propeller calculated by BEM can be used as a surface force to exert on the finite element structure, and can be equivalently shifted to the element nodes by Formula (26).

$$\boldsymbol{F}_{\mathrm{r}}^{\mathrm{e}}=\iint_A \boldsymbol{N}^{\mathrm{T}}\boldsymbol{P}^{\mathrm{e}}\mathrm{d}A \tag{26}$$

Thus, the equivalent nodal force matrix $\boldsymbol{F}^{\mathrm{e}}$ of element in the basic equation of element $\boldsymbol{K}^{\mathrm{e}}\boldsymbol{u}^{\mathrm{e}}=\boldsymbol{F}^{\mathrm{e}}$ can be obtained.

$$\boldsymbol{F}^{\mathrm{e}}=\boldsymbol{F}_{\mathrm{ce}}^{\mathrm{e}}+\boldsymbol{F}_{\mathrm{r}}^{\mathrm{e}} \tag{27}$$

In the formula: $\boldsymbol{F}_{\mathrm{ce}}^{\mathrm{e}}$ and $\boldsymbol{F}_{\mathrm{r}}^{\mathrm{e}}$ are the centrifugal force and the hydrodynamic load on the element respectively.

3 Calculation process

Using the bidirectional fluid–solid coupling method, that is, the calculation result predicted by BEM and the structure calculation result predicted by FEM can be transferred between each other, and the two methods started a new calculation in the iteration because of the change of boundary conditions. Information was transferred back and forth in the fluid and structural modules until the solution satisfying the convergence condition was obtained. Fig. 5 shows the flow chart of calculation in this paper, and the iterative process is as follows:

1) In low–order BEM based on velocity potential, a perturbation velocity potential ϕ was obtained by solving Formula (1) for the hyperboloid elements arranged by each blade, and the pressure distribution and hydrodynamic performance of the control points of surface element were obtained by the Bernoulli equation.

2) The centrifugal force caused by the surface pressure distribution and structural element rotation of propeller was applied to the volume element of finite element. Through the total force balance equation (11) of the whole structure, the distribution of stress and displacement of the propeller was calculated.

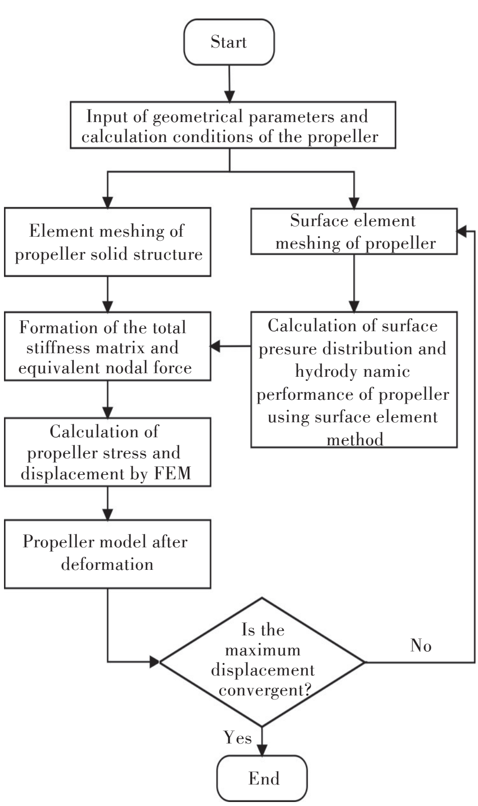

Fig.5 Calculation process of fluid–solid interaction for propeller

3) The surface node displacement of the propeller calculated by FEM was added to point coordinates of BEM. The perturbation velocity potential ϕ was obtained by solving Formula (1), and pressure distribution and hydrodynamic performance of surface element control points were obtained by using the Bernoulli equation.

4) Steps 2) and 3) were repeated until the maximum displacement convergence condition was satisfied.

4 Calculation model and parameter setting

In this paper, the DTRC 4119 model propeller was taken as the research object, the influence of mesh number and meshing on the calculation results was investigated, and the feasibility of the proposed method was evaluated. The propeller diameter was 0.305 m, the hub diameter ratio was 0.2, there was no pitch or skew, and the section profile was NACA–66mod. The nickel–aluminum bronze with a density of 7 600 kg/m^3 was selected as material of the propeller, the elastic modulus of it was E=113 GPa, and Poisson's ratio was μ =0.34. In view of the rigid connection between the propeller blades and the propeller hub, rigid constraint of six degrees of freedom on the nodes of blade root was carried out in the model for the convenience of calculation. The calculation conditions were set as follows: the design advance coefficient was 0.833, and the rotational speed was 600 r/min.

5 Mesh number and convergence analysis

According to the previous practice and research in finite element, it is found that the mesh size of solid structure will directly affect the accuracy of the calculation results. In this section, with reference to the correlation research method, influence of the propeller with different mesh numbers on the calculation results was predicted, and the calculation data were fully explored, so as to grasp the correlation between the calculation results and variables, which was used to guide the selection of the proper propeller mesh number to make the calculation results more accurate and not affect the calculation speed in the meantime.

5.1 Span–wise and chord–wise mesh numbers

Based on the above method, 10 kinds of meshing methods were adopted, namely, the chord-wise and span-wise mesh numbers of 10 × 10, 12 × 12, 14 × 14, 16 × 16, 18 × 18, 20 × 20, 22 × 22, 24 × 24, 26 × 26 and 28 × 28. The mesh number of the thickness direction was fixed at 6, and then the results were analyzed.

Figs. 6 and 7 are respectively the distribution of blade stress and displacement obtained by importing the prediction results of blade stress into the Tecplot software, that is, in the calculation conditions, the stress and displacement distribution of blade surface when the chord-wise and span-wise mesh numbers were 12 × 12, 16 × 16 and 20 × 20, respectively. In the prediction, the same contour value range was set up for comparison. It can be seen from Fig. 6 that with the increase of mesh number, the blade stress continued to increase and the blade stress distribution became more uniform; when the mesh number was too small, the blade stress peak tended to be concentrated at a certain point. It can be seen from Fig. 7 that the trend of blade displacement distribution was basically the same under different mesh numbers, but the difference of displacement was larger.

In order to better analyze the effect of chord-wise and span-wise mesh numbers on the convergence of the calculation results, Fig. 8 shows the maximum equivalent stress and the maximum displacement corresponding to different chord-wise and span-wise mesh numbers in calculation conditions. We can see from Fig. 8, with the increase of mesh number, the

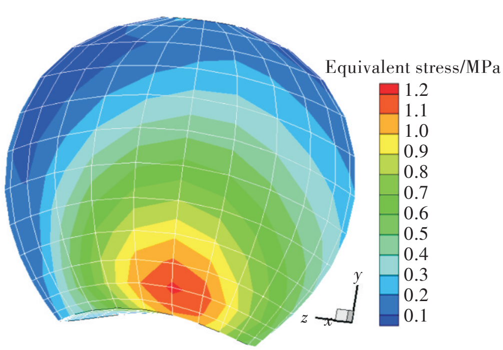

(a) Mesh number of 12×12

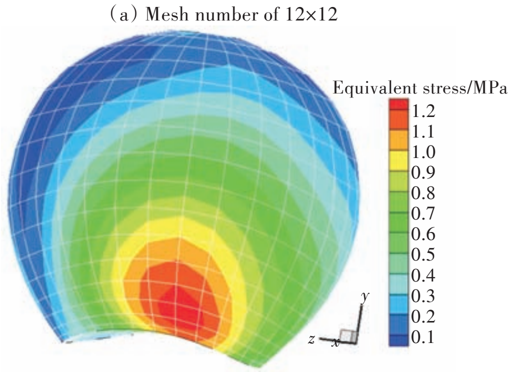

(b) Mesh number of 16×16

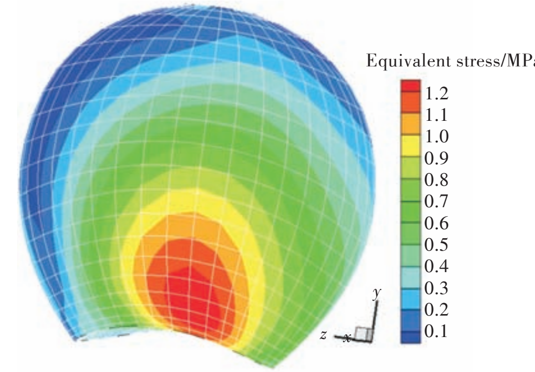

(c) Mesh number of 20×20

Fig.6 Equivalent stress distributions of blade with different chord-wise and span-wise mesh numbers

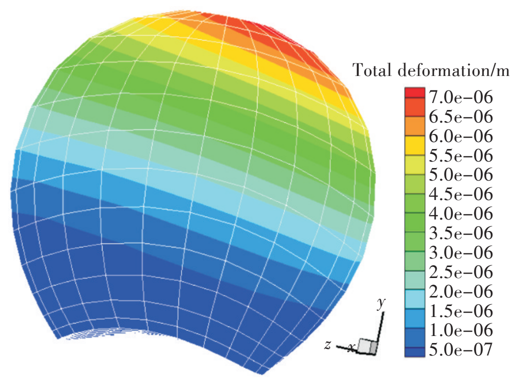

(a) Mesh number of 12×12

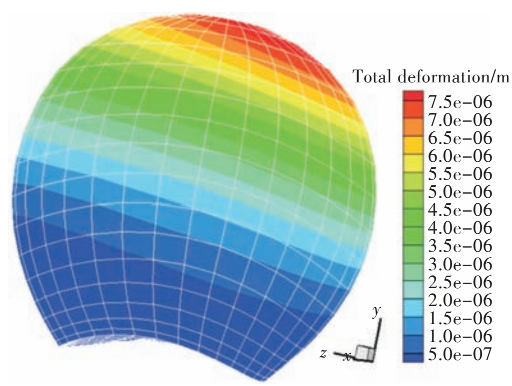

(b) Mesh number of 16×16

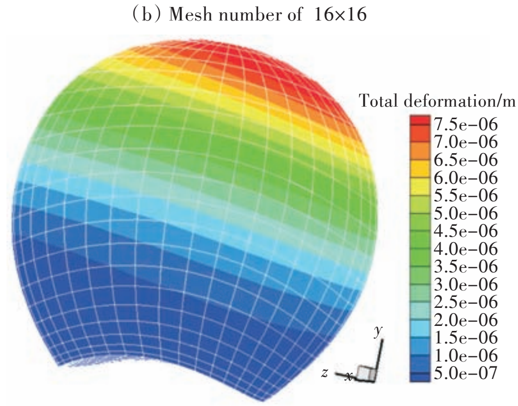

(c) Mesh number of 20×20

Fig.7 Displacement distributions of blade with different chord-wise and span-wise mesh numbers

maximum equivalent stress and the maximum displacement increased continuously, but the amplitude of increase decreased; when the mesh number reached 24, the maximum equivalent stress and the maximum displacement still showed a growth trend, but the amplitude of increase was very small. Therefore, when the chord-wise and span-wise mesh numbers were 24 × 24, the results can be considered convergent basically.

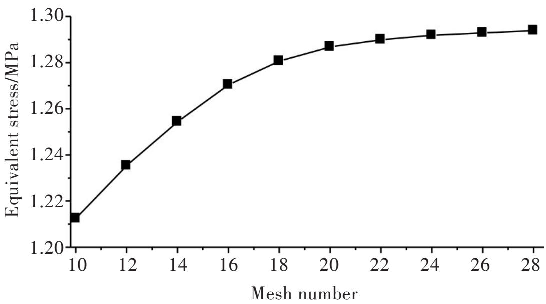

(a) Maximum equivalent stress of blade

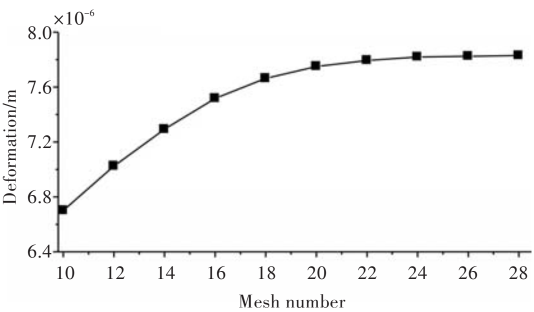

(b) Maximum displacement of blade

Fig.8 Convergence process with different chord-wise and span-wise mesh numbers

5.2 Mesh number in thickness direction

Based on the above method, the calculation results were analyzed when the mesh numbers in thickness direction were 2, 3, 4, 5, 6, 7, 8, respectively, and the chord-wise and span-wise mesh numbers were fixed to 24 × 24. The mesh number in thickness direction has influence only on finite element meshing, but not affects meshing of BEM. Therefore, before the fluid-solid coupling iteration, the calculation results of the hydrodynamic performance of mesh number in different thickness directions were the same.

Figs. 9 and 10 show the blade stress and displacement distributions at the mesh number of 2, 4 and 6 in thickness direction under the calculation conditions. For the convenience of comparison, the same contour value range was set. It can be seen from Fig. 9 that mesh number in thickness direction has a great influence on the calculation results of blade stress. With the increase of mesh number, the range of red region was larger and larger, which indicates that the stress of blade shows an overall increasing trend. It can be seen from Fig. 10 that the distribution trend of blade displacement calculated by different mesh numbers was basically the same, but with the increase of mesh number, the red region became larger, indicating that the blade displacement also shows an overall increasing trend. It can be seen that the mesh number in thickness direction has a great influence on the calculation results of propeller strength.

In order to better analyze the influence of chord-wise and span-wise mesh numbers on the convergence of the calculation results, Fig. 11 shows the maximum equivalent stress and displacement obtained at different mesh numbers in thickness direction under the calculation conditions. As shown in Fig. 11, with the increase of mesh number, the maxi-

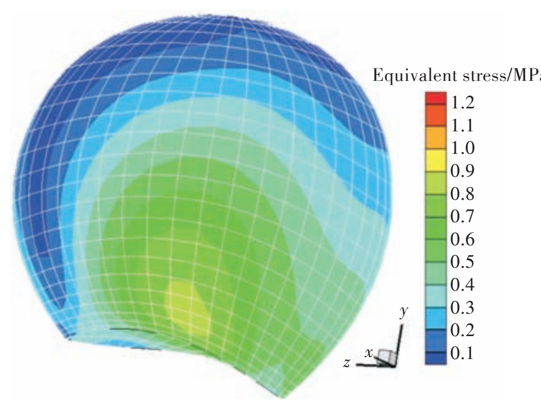

(a) Mesh number of 2

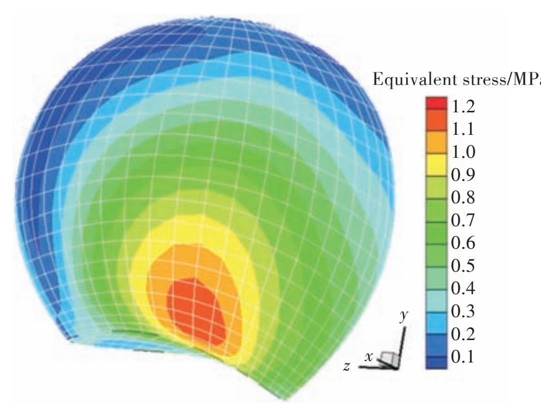

(b) Mesh number of 4

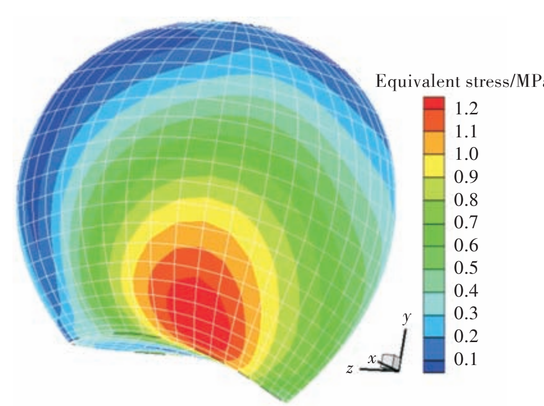

(c) Mesh number of 6

Fig.9 Equivalent stress distributions of blade with different mesh numbers in thickness direction

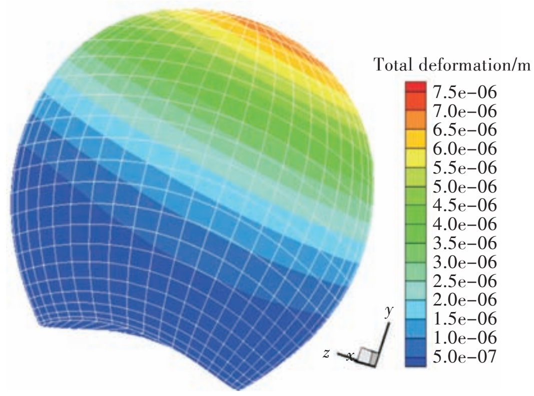

(a) Mesh number of 2

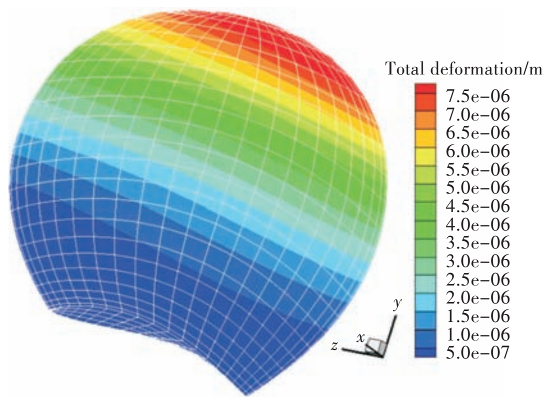

(b) Mesh number of 4

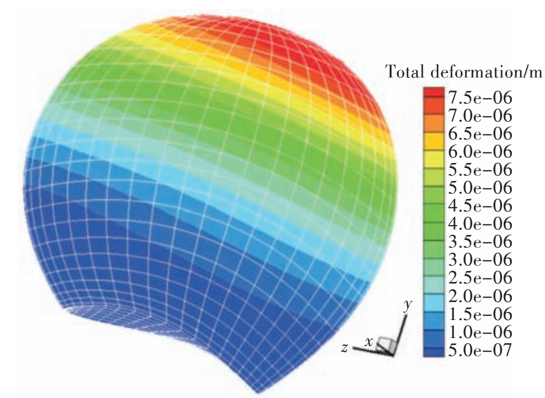

(c) Mesh number of 6

Fig.10 Displacement distributions of blade with different mesh numbers in thickness direction

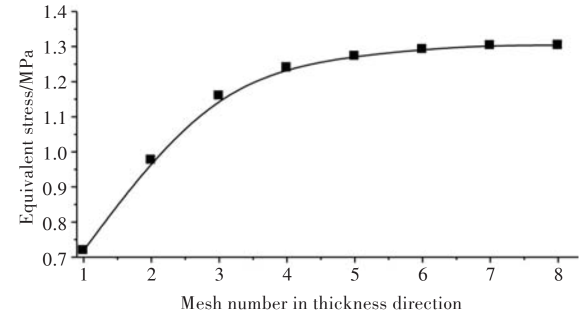

(a) Aximum equivalent stress of blade

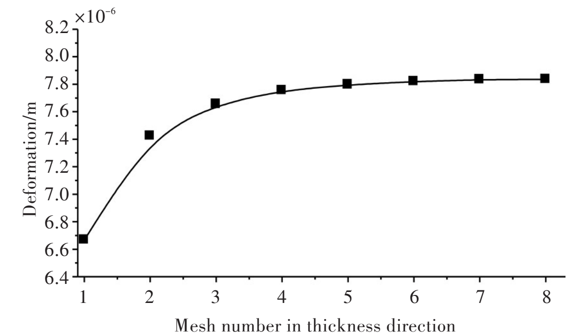

(b) Maximum displacement of blade

Fig.11 Convergence process with different mesh numbers in thickness direction

mum equivalent stress and displacement increased continuously, but the amplitude of increase decreased rapidly. So, when the mesh number increased to more than 6, the calculation results can be basically considered convergent.

6 Method validation

There have been many references [16-18] verifying the calculation accuracy of steady hydrodynamic performance of propeller by BEM, which would be no longer detailed in this paper. In this paper, we focused on the calculation accuracy of propeller strength using the FEM/BEM coupled method proposed in this paper, that is, the calculation results of propeller strength were mainly analyzed and verified.

In order to verify the accuracy of the proposed method in predicting propeller strength, the stress prediction results in this paper were compared with those in Ref. [19]. According to the above mesh number and convergence analysis, semi-cosine division was adopted for the chord-wise and span-wise directions of the propeller surface, and the chord-wise and span-wise mesh numbers were 26 × 26 when BEM was used to calculate the steady hydrodynamic performance of the propeller. In the calculation conditions, the thrust coefficient and torque coefficient were 0.143 2 and 0.026 5 obtained by the BEM calculation program in this paper, 0.135 2 and 0.028 1 calculated by Ref. [19] respectively, and 0.141 2 and 0.027 8 measured by model test [20]. Thus, compared with the thrust and torque coefficients measured by model test, the calculation results by the proposed method were close to the measured results; compared with the results of Ref. [19], the thrust coefficient calculated by the proposed method was larger than that in Ref. [19], and the torque coefficient was smaller than that in Ref. [19].

In the static strength analysis of FEM on the propeller, the chord-wise and span-wise directions of the propeller solid structure were the same as those of BEM, and the mesh number was 8 in thickness direction by average meshing.

The stress distribution of the blade back and surface of the DTRC 4119 model propeller obtained by the proposed prediction method is shown in Fig. 12. By comparing it with the distribution results calculated in Ref. [19], it is found that the trend of blade stress distribution calculated by the proposed method was basically consistent with that in Ref. [19]. The check of propeller strength mainly focused on whether the maximum equivalent stress was more than the allowable stress. The maximum equivalent stress of blade calculated in this paper was 1.31 MPa, and that predicted by Ref. [19] was 1.18 MPa, which shows that the prediction results of the proposed method were larger than those of Ref. [19]. Although there was a certain deviation between the maximum equivalent stress values calculated by the two methods, they were still reasonable from the magnitude. There are many reasons for the deviation in the calculated results, including: the pressure distribution of hydrodynamic load of propeller predicted by BEM and CFD method cannot be the same; the type and number of finite element meshing by the two methods were different; and load in the two methods was applied and transferred in different ways. It should be also noted that the blade stress calculated by the proposed method was concentrated in the middle part of the chord-wise blade root, which is consistent with the conclusion obtained in Ref. [19].

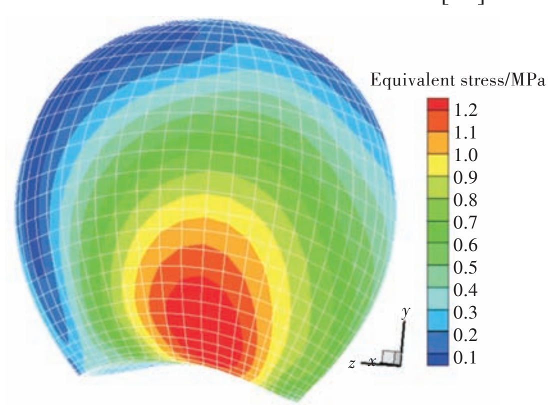

(a) Blade back

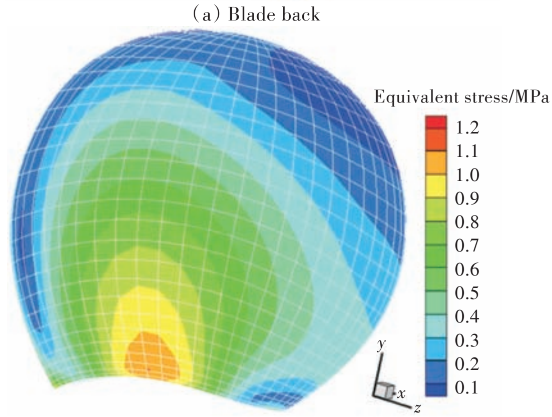

(b) Blade surface

Fig.12 Equivalent stress distributions of blade

The displacement distribution of the blade back and surface of the DTRC 4119 model propeller predicted by the proposed method is shown in Fig. 13. As shown in Fig. 13, the displacements of the blade surface and the blade back were the same. The stress distribution calculated by the proposed method was consistent with the results calculated in Ref. [19]. The blade displacement mainly affects the hydrodynamic performance of the propeller. Because the propeller model is rigid propeller, and the displacement is small, it will not cause the change of hydrodynamic force. The maximum displacement of blade calculated in this paper was 7.92×10^{-6} mm, and the maximum displacement predicted by Ref. [19] was 7.0×10^{-6} mm, which shows that the predicted value in this paper was somewhat larger.

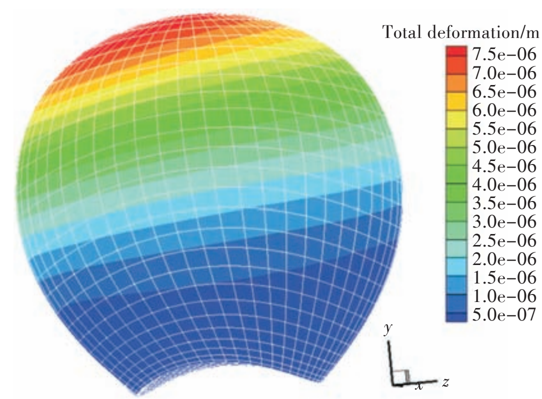

(a) Blade back

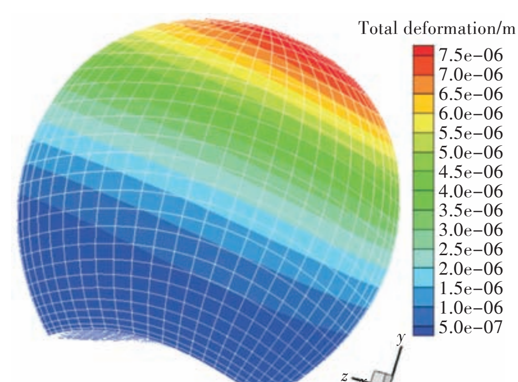

(b) Blade surface

Fig.13 Displacement distributions of blade

In view of the fact that the propeller strength is mostly checked by the cantilever beam method in China, the check results of the proposed method were compared with those of the cantilever beam method to verify the credibility of the proposed method. In Ref. [4], a prediction method of blade stress distribution with coupled cantilever beam and BEM was proposed. Because of the limitation of cantilever beam, it is difficult to predict the displacement of blade. Fig. 14 shows the blade stress distribution of the DTRC 4119 model propeller predicted by Ref. [4] under the same working conditions with those in this paper. By comparing Figs. 12 with 14, the trend of the blade stress distribution calculated by the proposed method was similar to the results by the cantilever beam method, and the maximum stress of blade was concentrated in the center of the blade root, but the maximum value of blade stress had certain differences. Wherein, the maximum tensile stress of blade predicted by the cantilever beam method was 1.03 MPa, which was smaller than the result calculated by the proposed method. The cause of the deviation was that the cantilever beam method over simplified the blades; the strength theories of the two methods differed. The cantilever beam method uses the maximum tensile stress theory (the first strength theory), and the proposed method uses the energy theory of shape change (the fourth strength theory).

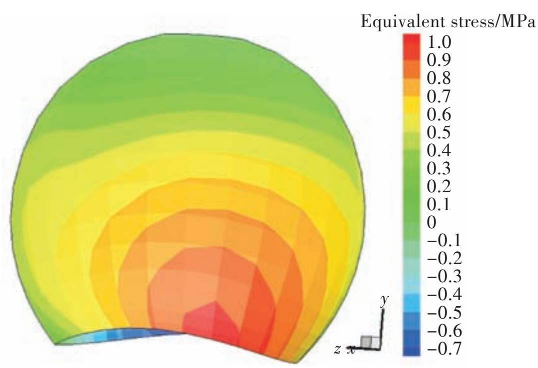

(a) Blade back

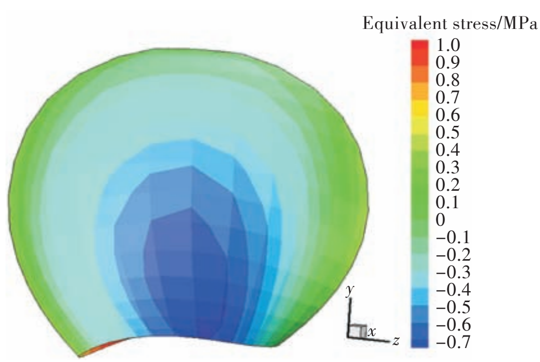

(b) Blade surface

Fig.14 Stress distributions of DTRC 4119 blade predicted by the cantilever beam method

In order to verify the applicability of the proposed method to highly skewed propeller, stress distribution and displacement distribution of blade with a skewed angle of 36° were predicted, with the results shown in Fig. 15. It can be seen from the figure that the maximum stress of blade occurred at the blade root close to the following edge, which is consistent with the conclusions obtained in Ref. [8].

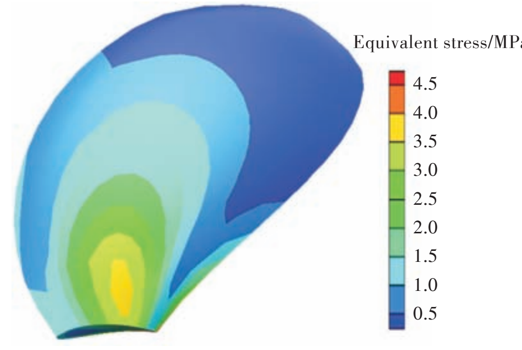

(a) Stress distribution of blade back

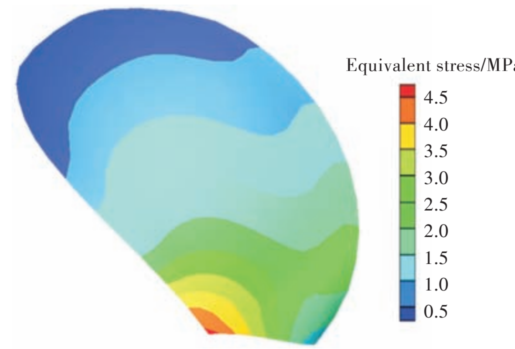

(b) Stress distribution of blade surface

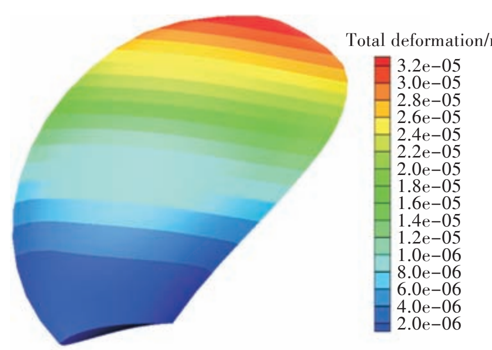

(c) Stress distribution of blade surface

Fig.15 Stress and displacement distributions of DTRC 4382 predicted by current method

7 Conclusions

In this paper, related theory of FEM was introduced to solve the static strength of propeller, and a method of finite element structural element division of propeller and BEM/FEM coupled prediction of static strength of propeller was proposed and studied. The influence of different mesh numbers of blades in span-wise, chord-wise thickness directions on the calculation results and convergence was discussed, and the calculation results of this method were compared with those of related references, which verified the feasibility of the proposed method. The object of calculation was analyzed and the following conclusions were obtained:

1) The analysis of the effect of different mesh numbers of chord-wise and span-wise blades on the re-

sults shows that: with the increase of mesh number, the blade stress distribution was more uniform, the maximum equivalent stress and the maximum displacement showed an increasing trend, but the amplitude of increase decreased rapidly, and the results can be convergent only when the mesh number of chord-wise and span-wise blades reached over 26 × 26.

2) The analysis of the effect of different mesh numbers of blade in thickness direction on the results shows that: with the increase of mesh number, blade stress and displacement showed an overall increasing trend, but the amplitude of increase decreased rapidly, and the results can be convergent only when the mesh number in thickness direction reached over 6.

3) The stress and displacement distributions of blade calculated by the proposed method were in good agreement with the calculation results of relevant references, indicating that the proposed method is simple and fast, and the calculation accuracy can be ensured.

It is easy to analyze the static strength of propeller using the proposed method, and it can quickly calculate the stress and displacement distribution of propeller blade. In the follow-up research, it will be applied in other types of propellers to further verify the proposed method, and the program would be embedded into the theoretical design and optimization design process of propellers, so as to improve the strength assessment and computational efficiency of propeller in the design stage.

References

[1] BOSWELL R J. Static stress measurements on a highly-skewed propeller blade[R]. Washington, DC: Naval Ship Research and Development Center, 1969.

[2] ZHAO B. 大侧斜螺旋桨强度研究[D]. Wuhan: Huazhong University of Science and Technology, 2003 (in Chinese).

[3] YANG X H, CHENG E S. Study on stress measurement of the high skewed propeller blades[J]. Ship & Ocean Engineering, 2004(1): 6-9 (in Chinese).

[4] YE L Y, WANG C, SUN S, et al. Prediction of blade stress distribution based on cantilever beam method and panel method[J]. Journal of Wuhan University of Technology (Transportation Science & Engineering), 2015(5): 968-973 (in Chinese).

[5] HUANG Y, XU H, JIANG Z F. Strength analysis of highly-skewed propeller[J]. Chinese Journal of Ship Research, 2010, 5(5): 44-48 (in Chinese).

[6] LIU Z C. 船用螺旋桨的数值模拟及流固分析[D]. Zhenjiang: Jiangsu University of Science and Technology, 2012: 1-8(in Chinese).

[7] CHEN Y, ZHU X, HUANG Z, et al. Strength evaluation of the composite propeller under hydrodynamic fluid load[J]. Chinese Journal of Ship Research, 2015, 10(1): 19-26 (in Chinese).

[8] SUN H T, XIONG Y. Study on hydrodynamic and deformation performance of propellers considering the blade deformation[J]. Journal of Harbin Engineering University, 2013, 34(9): 1108-1112, 1118 (in Chinese).

[9] HU S G, WANG G Q, WANG X B. Thick shell element method of stress analysis of propeller blades[J]. Journal of Shanghai Jiaotong University, 1988, 22(2): 33-42 (in Chinese).

[10] WANG Y H. Comparative studies on highly-skewed propeller strength [J]. Journal of Ship Mechanics, 1998, 2(2): 44-51 (in Chinese).

[11] LIU Z Q, CHEN Y H, YAO Z C. Static strength analysis of civil ship propellers[J]. Shipbuilding of China, 2012, 53(Supp 1): 25-30 (in Chinese).

[12] SU Y M, HUANG S. 船舶螺旋桨理论[M]. Harbin: Press of Harbin Engineering University, 2003 (in Chinese).

[13] XIAO C, QIN W J, ZUO Z X. Influence of element-form and element-size on FE calculation of crankshaft stress field[J]. Diesel Engine, 2004(Supp 1): 176-178 (in Chinese).

[14] LIAO H W. All-hexahedral mesh generation by iterative method [D]. Hangzhou: Zhejiang University, 2013: 20-34 (in Chinese).

[15] ZHAO J H, WANG M F. 弹性力学及有限元 [M]. Wuhan: Wuhan University of Technology Press, 2003: 18-20 (in Chinese).

[16] SU Y M, HUANG S. Prediction of hydrodynamic performance of marine propellers by surface panel method [J]. Journal of Harbin Engineering University, 2001, 22(2): 1-5 (in Chinese).

[17] HU J. Research on propeller cavitation characteristics and low noise propeller design [D]. Harbin: Harbin Engineering University, 2006 (in Chinese).

[18] WANG C. The research on performance of propeller's hydrodynamics, cavitation and noise [D]. Harbin: Harbin Engineering University, 2010 (in Chinese).

[19] GU C Z, ZHENG B L. Numerical analysis of propeller open-water performance and stress distribution in the blade of ship propeller[J]. Chinese Quarterly of Mechanics, 2011, 32(3): 440-443 (in Chinese).

[20] TAN T S. Performance prediction and theoretical design research on propeller in non-uniform flow [D]. Wuhan: Wuhan University of Technology, 2003 (in Chinese).

[*Continued on page* 58]